JAAS

PAPER

View Article Online
View Journal | View Issue

Cite this: *J. Anal. At. Spectrom.*, 2023, **38**, 1874

Unraveling the role of aerosol transport on nanomaterial characterization by means single particle inductively coupled plasma mass spectrometry†

Daniel Torregrosa, Guillermo Grindlay, Luis Gras and Juan Mora

Nanomaterials (NMs) characterization by means single particle inductively coupled plasma mass spectrometry (spICP-MS) relies on assessing transport efficiency. To this end, different strategies have been proposed but contradictory reports could be found about which strategy provides the most accurate results since our knowledge about NMs transport through the sample introduction system is still limited. The goal of this work is to evaluate the role of aerosol transport on NMs characterization by means spICP-MS. To this end, a 70 nm platinum nanoparticles (PtNPs) suspension and a 10 ng mL^{-1} ionic Pt solution were analyzed under different operating conditions. Next, plasma and tertiary aerosol characteristics (*i.e.*, drop size distribution and transport rate of solvent, PtNPs and Pt ions) were checked to explain experimental findings. Our results shows that the number of events, PtNPs event intensity and Pt ionic signal depend on both aerosol transport and plasma operating conditions. Interestingly, tertiary aerosol characterization reveals that NMs, ionic and solvent transport efficiencies differ significantly. Thus, irrespective of the nebulization conditions, transport efficiencies follow the order solvent > ionic Pt > PtNPs. For instance, when operating a nebulizer gas flow of 0.9 L min^{-1} and a sample uptake rate of 300 μL min^{-1}, transport efficiency values were 5.77 ± 0.03, 3.89 ± 0.12 and 3.35 ± 0.06%, respectively. Similar results were observed operating different metallic NPs (*i.e.*, 50/150 nm AuNPs) and spray chamber designs (*i.e.*, Scott double pass/cyclonic spray chambers). These findings are of fundamental importance for spICP-MS metrology since some strategies for evaluating transport efficiency are based on assuming that the above-mentioned species are transported similarly into the plasma. The method based on the number of events seems the best approach since it is really based on NMs transport into the plasma. Both ionic and NMs pulse intensity ratios and solvent-based methodologies are, however, not based on NMs transport efficiency and, hence, they could lead to inaccurate NMs characterization in terms of particle size and concentration depending on spICP-MS operating conditions. For both approaches, because the dampening effect of cubic root when calculating particle size from transport efficiency, particle size distribution bias was less significant than particle concentration bias.

Received 27th April 2023
Accepted 25th July 2023

DOI: 10.1039/d3ja00134b

rsc.li/jaas

1. Introduction

Single particle inductively coupled plasma mass spectrometry (spICP-MS) is a powerful analytical tool for the characterization and quantification of nanomaterials (NMs) in a wide variety of samples.[1,2] In this technique, a diluted NMs suspension is nebulized, and the aerosol generated is transported through the spray chamber to the plasma, where NMs are vaporized/atomized and their constituting atoms are ionized, generating an ion cloud. If transient signals are registered, each ion cloud generates a signal peak (*i.e.*, particle event over a continuous baseline). Operating this way, the number of events detected in a spectrum and their intensity can be related to particle concentration and mass, respectively.[3,4]

Over the years, a significant number of works have investigated technique fundamentals and how certain experimental parameters affect NMs characterization, such as: (i) plasma operating conditions (r.f. power, nebulizer gas flow rate, integration time, *etc.*);[5–7] (ii) NMs physicochemical properties;[8,9] (iii) sample introduction system;[10,11] (iv) spectral interference reduction by means collision/reaction technology;[12–14] (v) non-spectral interferences by inorganic[15–18] and organic matrices;[17,19,20] (vi) calibration strategies;[18,19,21–23] and (vi) mass analyzer detection capabilities.[24] Though these efforts have significantly improved technique metrology, there are still gaps

University of Alicante, Department of Analytical Chemistry, Nutrition and Food Sciences, PO Box 99, 03080 Alicante, Spain. E-mail: guillermo.grindlay@ua.es

† Electronic supplementary information (ESI) available. See DOI: https://doi.org/10.1039/d3ja00134b

in the state-of-the-art, particularly about NMs transport through the sample introduction system under different nebulization conditions and how this affects NMs characterization.

In the absence of certified NMs standard suspensions of known particle concentration and size, NMs determination is accomplished by estimating NMs transport efficiency (*i.e.*, the fraction of aspirated NMs reaching the plasma).[25–27] To this end, different strategies have been proposed in the literature: (i) number of events. A suspension of known concentration is nebulized, and transport efficiency is estimated from the ratio between the number of particles detected with respect to those initially nebulized. While this strategy is specifically based on NMs transport into the plasma, special care is required selecting experimental conditions and signal processing algorithms to differentiate NMs ionization signal from the background;[3] (ii) ionic and NMs pulse intensity. In this approach, transport efficiency is estimated by using both an ionic and a NMs (generally NPs) standard suspension of known mean diameter. Assuming that ions and particles behave similarly through the analysis by means spICP-MS (*i.e.*, nebulization, transport, and ionization), NMs transport efficiency is estimated as the quotient of signal-to-mass ratios of both the ionic standard and the NMs standards;[25] and (iii) solvent transport methodologies.[25,28,29] Nanomaterials transport efficiency is evaluated by measuring the aerosol mass introduced into the plasma with regard the sample amount nebulized for a given period of time (*e.g.*, 60 min). This strategy assumes that both NMs and solvent are transported into the plasma equivalently.

Though these approaches have been successfully employed in a wide range of analytical applications, contradictory reports are found in the literature about which one is the most suitable for the accurate and precise characterization of NMs by means spICP-MS.[4,27] For instance, some authors have observed that transport efficiency estimated by using intensity signals is usually higher (10–40%) than that obtained with the number of events.[26,30] However, it has also been reported that both approaches provide equivalent results.[25] As regards solvent-based methodologies, it has also been noted that they usually overestimate transport efficiency with regard the remaining approaches.[25,26] This lack of consistency is not surprising considering that any of the above-mentioned strategies are based upon a series of hypothesis (*i.e.*, NMs, ions and solvent do behave equivalently through the sample introduction system and within the plasma)[31–34] which might not be always fulfilled thus providing biased results.

The limited number of studies about aerosol transport fundamentals with spICP-MS can be attributed to the lack of a direct methodology for assessing NMs transport. Our research group has recently demonstrated that this parameter can be directly measured using a similar procedure to that previously described for assessing dissolved ions transport efficiency.[35] This procedure is based on aerosol retention at the exit of the spray chamber with the aid of microquartz filters followed by a microwave-assisted extraction treatment with ammonium hydroxide 2% w w^{-1} and NMs quantification by spICP-MS. Therefore, this procedure allows, together with well-stablished protocols for solvent and dissolved ion transport rate measurements,[36] investigate aerosol transport phenomena influence on spICP-MS figures of merit. The goal of this work was to evaluate the influence of the methodology selected for transport efficiency estimation on NMs characterization by means spICP-MS and to gain insight into the differences on transport efficiencies provided by each methodology. To this end, a 70 nm platinum nanoparticles (PtNPs) suspension and an ionic Pt solution were analyzed under different operating conditions (*i.e.*, nebulizer gas flow, Q_g; sample uptake rate, Q_l; and sampling depth positions, SD) by means spICP-MS using a liquid sample introduction system made of a MicroMist concentric pneumatic nebulizer and a Scott double pass spray chamber. Next, plasma characteristics (CeO^+/Ce^+ ratio) and tertiary aerosols (*i.e.*, drop size distribution and transport rate of solvent, PtNPs and Pt ions) were checked to explain signals afforded by spICP-MS. After that, current methodologies for estimating transport efficiency and NMs characterization were critically reviewed considering experimental results. In order to validate major experimental findings, alternative metallic NPs (*i.e.*, 50 and 150 nm AuNPs) and spray chamber design (*i.e.*, cyclonic) were additionally tested.

2. Materials and methods

2.1. Reagents and materials

All solutions and suspensions were prepared using ultrapure water (Milli-Q water purification system, Millipore Inc., Paris, France). A stock suspension of citrate-stabilized PtNPs with a nominal diameter of 70 nm and a nominal concentration of 1.2×10^{10} mL^{-1} (NanoComposix, San Diego, USA) and citrate-stabilized AuNPs with nominal diameters of 50 and 150 nm and concentrations of 3.5×10^{10} and 3.6×10^{9} mL^{-1} (Cytodiagnostics, Burlington, Canada) were employed through this work. Similarly, Pt and Au mono-elemental 1000 mg L^{-1} standards (Sigma-Aldrich, Schelldorf, Germany) were employed to assess ionic aerosol transport as well as to characterize metallic NMs. A Ce mono-elemental 1000 mg L^{-1} standard (Sigma-Aldrich, Schelldorf, Germany) was diluted to evaluate plasma characteristics under different operating conditions (*i.e.*, CeO^+/Ce^+ ratio). Silica gel was used to evaluate solvent transport efficiency (Sigma-Aldrich, Schelldorf, Germany). Microquartz-fiber filters (50 mm diameter, 0.3 mm nominal pore size, Munktell) from Thermo-Fisher Scientific (Waltham, USA) were used for measuring PtNPs transport efficiency through the sample introduction system. Ammonium hydroxide solution (28% w w^{-1}) and ultrapure nitric acid (69% w w^{-1}) from Sigma-Aldrich (Steinheim, Germany) were, respectively, employed to prepare PtNPs and ionic Pt extracting media from microquartz-fiber filters.

2.2. Instrumentation

A triple quadrupole-based 8900 ICP-MS instrument (Agilent, Santa Clara, USA) was employed throughout this work for assessing the influence of working conditions on NPs characterization by means spICP-MS. This instrument was equipped with a MicroMist concentric pneumatic nebulizer and a Scott double pass spray chamber (inner volume 75 cm^3) cooled at 2 °C

(Agilent, Santa Clara, USA). Nevertheless, additional experiments were performed using a cyclonic spray chamber (inner volume 42 cm^3) instead of the double pass one. Table 1 summarizes ICP-MS operating conditions. In all cases, metallic NMs suspensions were sonicated for 1 min prior to ICP-MS measurements using a 50 W ultrasound water bath (Selecta, Barcelona, Spain). Data acquisition and analysis were conducted *via* the single nanoparticle application module present in the software controlling ICP-MS (MassHunter version 4.5). Separation of event signals from background was carried out by defining a signal threshold as 5 times the standard deviation of the background signals (*i.e.*, 5σ criterion).[3]

Prior to ICP-MS measurements, NMs were characterized by means transmission electron microscopy (TEM), using a JEM-1400 Plus electron microscope (JEOL, Tokio, Japan) operating at 120 kV. Nanoparticle size distribution data afforded by TEM were employed as a reference for evaluating instrumental conditions effect on particle size distributions. A detailed description of sample preparation procedure for TEM observations can be found elsewhere.[35]

2.3. Characterization of tertiary aerosols

In this work, a thorough characterization of tertiary aerosols at the exit of the spray chamber was performed under different Q_g and Q_l (Table 1). To this end, the following parameters have been monitored: (i) tertiary aerosol drop size distribution; (ii) solvent transport rate; (iii) PtNPs transport rate; and (iv) ionic Pt transport rate.

2.3.1. Drop size distribution. Tertiary aerosols drop size distributions were measured by means of a Fraunhoffer laser diffraction system (model 2600c, Malvern Instruments Ltd., Malvern, Worcestershire, UK). A detailed description of instrument characteristics can be found elsewhere[36,37] (Fig. S1, ESI†).

2.3.2. Solvent transport rate. Solvent transport rate (S_{tot}) into the plasma was determined by collecting the aerosol at the exit of the spray chamber by means a U-tube filled with dried silica gel for 10 minutes[36,37] (Fig. S2, ESI†).

Table 1 ICP-MS operating conditions for the detection of dissolved ions and NPs

	Conventional mode	Single particle mode
Plasma forward power (W)	1550	
Sampling depth (mm)	4/8/12	
Argon flow rate (L min^{-1})		
Plasma	15	
Auxiliary	0.9	
Nebulizer (Q_g)	0.7/0.9/1.1	
Torch i.d. (mm)	1.0	
Sample introduction system		
Nebulizer	MicroMist®	
Spray chamber	Scott double pass & cyclonic	
Sample uptake rate (Q_l) (μL min^{-1})	100/300/500	
Dwell time (ms)	10	0.1
Measuring time (s)	5	60
Nuclides	$^{195}Pt^+$, $^{197}Au^+$	

2.3.3. PtNPs transport rate. Nanomaterial transport rate (W_{NP}) was assessed according to the procedure developed in a prior work.[35] Briefly, a 7×10^6 mL^{-1} PtNPs suspension was nebulized for 10 min and tertiary aerosols were collected at the exit of the spray chamber with the aid of a microquartz filter and a vacuum pump (Fig. S3, ESI†).

Next, filters were immersed into 40 mL of a 2% w w^{-1} NH_4OH solution and a set of 6 samples were heated inside a domestic microwave oven (Bluesky BMG20M-18) for 4 min using the highest power available (800 W). To avoid sample projections and minimize liquid loss by evaporation, samples were covered with a glass watch during the extraction process. Finally, the NMs extract was analyzed by means spICP-MS.

2.3.4. Ionic Pt transport rate. Ionic platinum transport rate (W_{ionic}) was measured using the same experimental procedure employed for assessing PtNPs transport rate (Fig. S3, ESI†). In this case, a 10 μg mL^{-1} ionic Pt solution was nebulized for 10 min. Because the poor solubility of Pt under basic conditions, a 1% w w^{-1} HNO_3 solution was employed to release ionic Pt from the microquartz filter.[36,43]

3. Results

Platinum nanoparticles were selected to gain insight about the role of aerosol transport on NMs characterization by means spICP-MS due to: (i) its high stability; (ii) the low memory effects shown by ionic solutions of Pt in ICP-MS; and (iii) the low complexity of Pt background spectrum. First, $^{195}Pt^+$ time scans afforded by a PtNPs suspension (1.5×10^4 mL^{-1}) were registered under different operating conditions (*i.e.*, Q_g, Q_l and SD). Next, both tertiary aerosol and plasma characteristics were examined to explain the changes noticed on spICP-MS signals. Plasma ionization conditions were indirectly evaluated by means the CeO^+/Ce^+ ratio[38] whereas tertiary aerosols were assessed by measuring: (i) aerosol drop size distribution; (ii) S_{tot}; and (iii) W_{NP}.[35,39] For the sake of comparison, signal changes for an ionic Pt solution (10 ng mL^{-1}) and W_{ionic} were also monitored. This information is highly valuable from a practical point of view since, in the absence of certified reference samples and standards, NMs characterization by means spICP-MS relies on the use of ionic standards.[25] Thus, it is important to evaluate whether NMs and dissolved ions behave similarly in spICP-MS.

3.1. Influence of operating conditions on the number of events and signal intensity for PtNPs

Considering previous studies in the literature about spICP-MS fundamentals,[6,31,32] the following variables were investigated: (i) Q_g (0.7/0.9/1.1 L min^{-1}); (ii) Q_l (100/300/500 μL min^{-1}); and (iii) SD (4/8/12 mm). The first two parameters control aerosol generation and transport but also affect plasma characteristics whereas the latter is critical to understand how NMs are atomized and ionized within the plasma. Radio frequency power was kept at 1550 W to favor atomization and ionization thus minimizing potential negative effects derived by solvent introduction into the plasma. Fig. 1 gathers the influence of Q_g

on both the number of events (Fig. 1a–c) and event signal intensity (Fig. 1d and e) for PtNPs under different Q_l and SD values.

3.1.1. Number of events. As shown in Fig. 1, the number of events peaked at a Q_g of 0.9 L min^{-1} for a SD of 4 mm (Fig. 1a) but it continually increased with Q_g when operating higher SDs (*i.e.*, 8 and 12 mm) (Fig. 1b and c). Irrespective of Q_g and SD, the number of events rose when increasing Q_l. For instance, at a SD of 4 mm and a Q_g of 0.7 L min^{-1}, the number of events for 100, 300 and 500 μL min^{-1} were, respectively, 210 ± 30, 320 ± 20 and 370 ± 20. Finally, it was also observed that, for a given set of Q_g and Q_l, the number of events was mostly independent of SD, except at 4 mm operating a Q_g of 1.1 L min^{-1}. Thus, when operating a Q_g of 0.9 L min^{-1} and a Q_l of 500 μL min^{-1}, pulses at SD of 4, 8 and 12 mm were 370 ± 20, 380 ± 20 and 360 ± 30, respectively.

Considering direct events dependence on the number of NPs transported into the plasma,[3,6,25] tertiary aerosols characteristics at the exit of the sample introduction system were systematically evaluated. Table 2 gathers tertiary aerosol mean diameter (D_{50}), S_{tot} and W_{NP} for different operating conditions. As expected from previous studies with pneumatic nebulizers,[40] D_{50} diminished with the increase of Q_g and when decreasing Q_l (Table 2). The higher the ratio between Q_g and Q_l, the higher energy per mass unit is available and hence finer aerosols are generated. Though differences on aerosol size were noticeable for some experimental conditions, there was not a clear relationship between tertiary aerosol D_{50} and the number of PtNPs events. Aerosol median diameter laid in a limited range (*i.e.*, 3.71 ± 0.02–4.38 ± 0.05 μm) and, hence, no significant differences on droplet vaporization/atomization should be expected. In addition, for all the conditions tested, droplets diameters were lower than 10 μm, maximum size undergoing complete desolvation when a conventional nebulizer-spray chamber is used (Fig. S4, ESI†).[41] Because signal behavior shown in Fig. 1a–

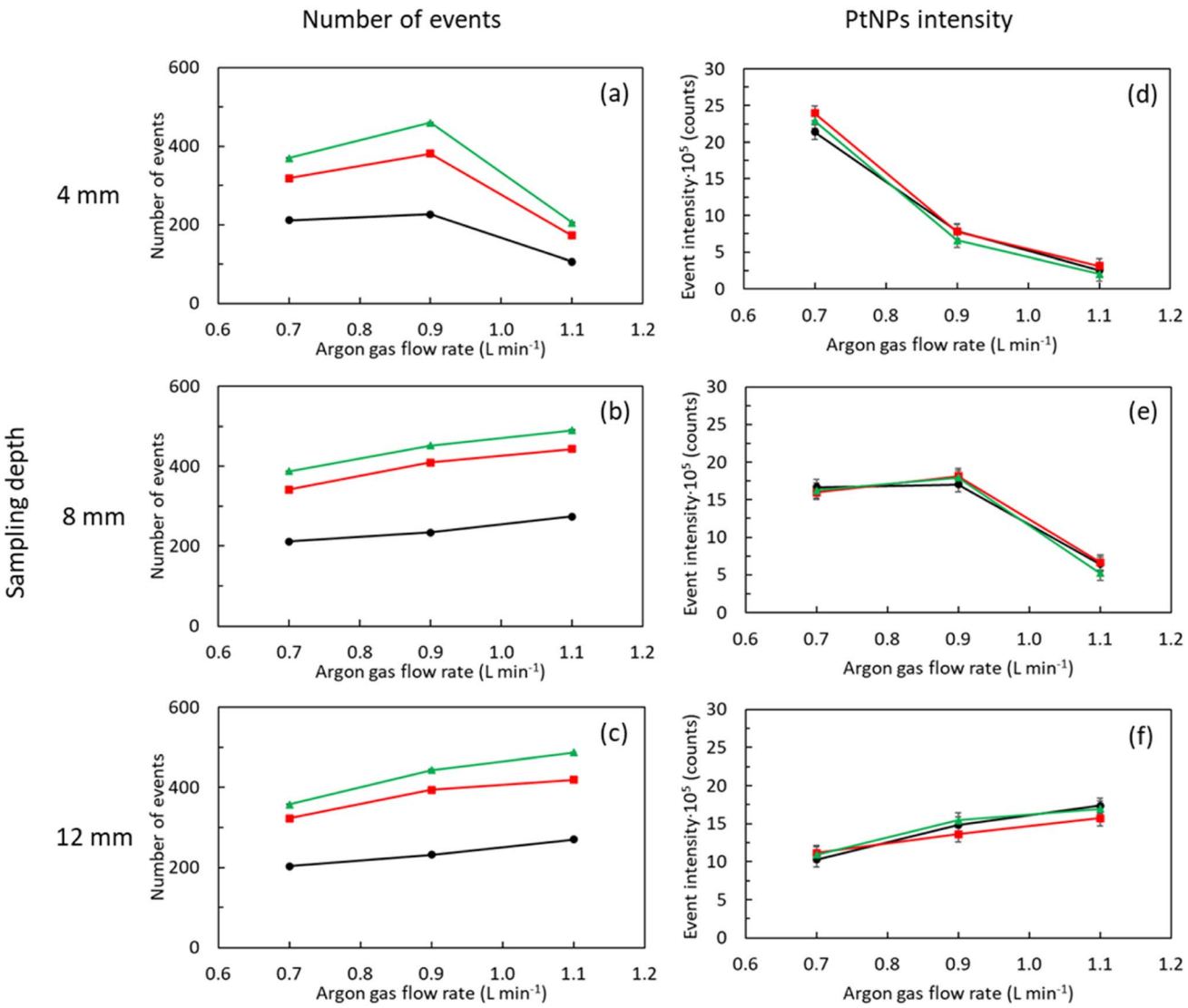

Fig. 1 Influence of the nebulizer gas flow rate on PtNPs number of events (a, b and c) and pulse signal intensity (d, e and f) at different SD and Q_l. Q_l: 100 (-●-), 300 (-■-), and 500 μL min^{-1} (-▲-); R.f. power: 1550 W; PtNPs concentration: 1.5 × 10^4 mL^{-1}.

Table 2 Influence of Q_g and Q_l on tertiary aerosol characteristics, solvent transport, PtNPs transport and ionic Pt transport

		Tertiary aerosol	Solvent	PtNPs	Pt ions
Q_g (L min^{-1})	Q_l (μL min^{-1})	D_{50} (μm)	S_{tot} (mg min^{-1})	W_{NP} 10^{-3} (part min^{-1})	W_{ionic} (μg min^{-1})
0.7	300	4.38 ± 0.05	14.77 ± 0.14	2.32 ± 0.04	2.56 ± 0.06
0.9	100	3.87 ± 0.03	10.0 ± 0.2	0.69 ± 0.02	1.03 ± 0.02
	300	3.96 ± 0.04	17.2 ± 0.1	2.37 ± 0.03	3.50 ± 0.11
	500	4.05 ± 0.04	20.6 ± 0.3	3.92 ± 0.10	6.8 ± 0.3
1.1	300	3.71 ± 0.02	15.8 ± 0.3	2.97 ± 0.03	4.5 ± 0.2

c cannot be explained in terms of aerosol size, additional factors should be considered such as S_{tot} and W_{NP} (Table 2). For a fixed Q_g (*i.e.*, 0.9 L min^{-1}), both S_{tot} and W_{NP} improved when increasing Q_l due to the higher sample amount introduced per unit of time.[37] Nevertheless, there were remarkable differences in the behavior of both factors when Q_g is modified for a given Q_l (*i.e.*, 300 μL min^{-1}). Thus, the former peaked at a Q_g of 0.9 L min^{-1} but the latter increased with Q_g. While the use of higher Q_g gave rise to finer aerosols (Table 2), aerosol velocity was also speeded up thus favoring droplet impact losses against spray chamber walls.[39,40] Because a diluted suspension was used, PtNPs might not be homogenously distributed on aerosol droplets and, hence, impact losses have a limited effect on W_{NP} when compared to S_{tot}, particularly if the NM was preferentially present on aerosol finest fraction. On this regard, it is important to remark that aerosol generated for a Q_g of 1.1 L min^{-1} showed a higher volume of smaller droplets than those obtained using Q_g values of 0.7/0.9 L min^{-1} (Table 2 and Fig. S4, ESI†). From these results, it can be concluded that S_{tot} does not properly reflect changes on NMs transport with Q_g.

If one considers results gathered in Fig. 1a–c and Table 2, it could be clearly observed that W_{NP} reflects pulse variations with both Q_g and Q_l. The lack of changes on pulse frequency with SD is not surprising given that, for a set of Q_g and Q_l, NMs transport rate is constant. Therefore, pulse suppression noticed at a SD of 4 mm and a Q_g of 1.1 L min^{-1} could only be attributed to changes on plasma atomization/ionization conditions.[19] To check this hypothesis, the CeO^+/Ce^+ ratio was monitored under different operating conditions (Fig. 2).[38] Irrespective of SD, this ratio increased with Q_g and Q_l, particularly for Q_g above 0.9 L min^{-1}. On the other hand, it was observed that oxide levels were enhanced when decreasing SD. On this regard, oxide levels were particularly high at a SD of 4 mm and a Q_g of 1.1 L min^{-1} (3×10^5–2.8×10^6%) thus confirming that pulse signal reduction is indeed related to a decrease on plasma robustness.[36] From these results, despite NM number of events are enhanced operating higher Q_g and Q_l, special care should be taken to avoid plasma deterioration, particularly due to its direct effect on NMs atomization/ionization.[19] On this regard, the CeO^+/Ce^+ ratio was only lower than 2% (*i.e.*, standard value for a robust plasma) when operating a Q_g of 0.7 L min^{-1}, regardless of Q_l and SD.

3.1.2. Signal intensity of PtNPs. As it is shown in Fig. 1d–f, PtNPs ionization signal strongly depended on both Q_g and SD. Irrespective of Q_l, when operating at a SD of 4 mm, pulse intensity significantly diminished (8-fold) when increasing Q_g from 0.7 to 1.1 L min^{-1}. However, the opposite was observed at a SD of 12 mm. In this latter case, event intensity enhancement with Q_g was rather limited (1.5-fold) when compared to signal changes noticed

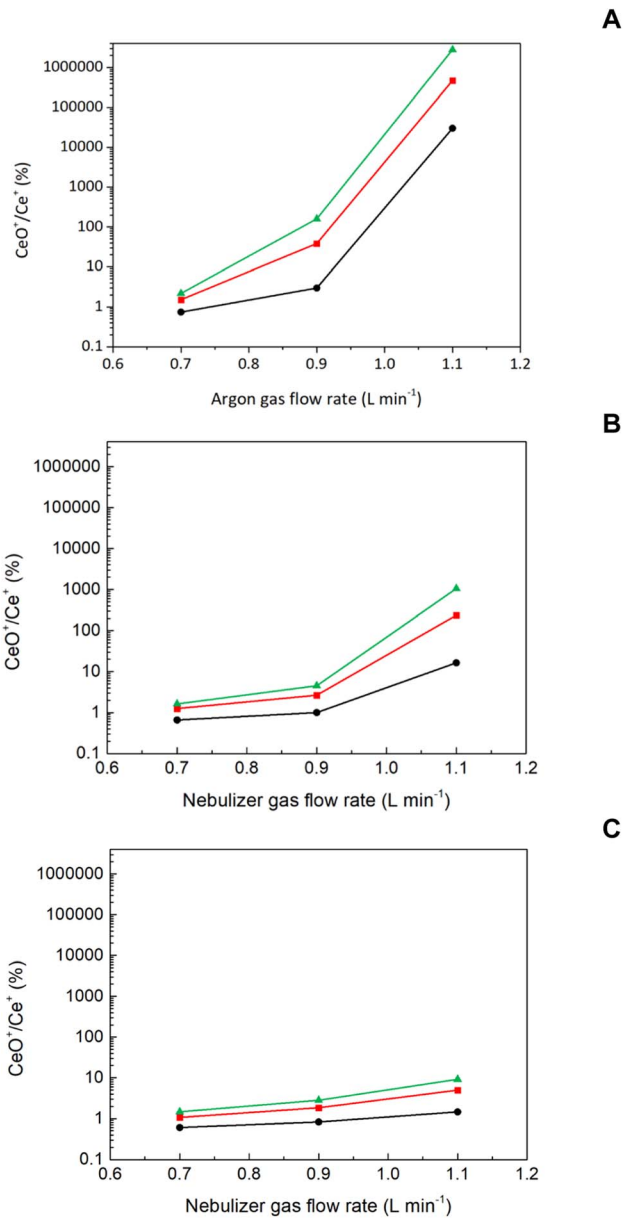

Fig. 2 Influence of the Q_g on the CeO/Ce^+ ratio at different Q_l and SD. Q_l: 100 (-●-), 300 (-■-), and 500 μL min^{-1} (-▲-); SD: 4 (A), 8 (B) and 12 mm (C); R.f. power: 1550 W.

at 4 mm. As regards the SD of 8 mm, event intensity showed an intermediate behavior to that outlined for 4 mm and 12 mm. To explain these findings, it should be considered how both plasma characteristics (*i.e.*, CeO^+/Ce^+ ratio) and Pt ionization are affected under different operating conditions (Fig. 2). The higher the oxide levels, the lower event signal was obtained thus remarking the influence of plasma robustness on NPs ionization. Interestingly, it was noticed that the highest event signal was achieved at 4 mm operating a Q_g of 0.7 L min^{-1}. For higher SD values (*i.e.*, 8 and 12 mm), the maximum pulse intensity was 1.5-fold lower to that obtained at 4 mm. These results suggest that the ion clouds generated by NPs ionization were more efficiently sampled at low SD thus minimizing ion diffusion off-axis and, hence, signal reduction.[31] From the results shown in Fig. 1d–f, Q_l did not exhibit a noticeable effect on event intensity. Signal intensity in ICP-MS depends on the total mass of analyte introduced into the plasma. A NP is either transported into the plasma or not and, hence, unless plasma conditions are severely deteriorated, signal intensity should be mostly independent of Q_l.[31]

3.2. Influence of operating conditions on ionic Pt signal intensity

In the same way as with the PtNPs suspension, an ionic Pt solution was analyzed (Fig. 3). Although this topic has been extensively covered in the literature over the years,[37] that kind of study is mandatory in the context of this work to investigate whether NMs and dissolved ionic species behave similarly under defined operating conditions. In general, the influence of operating conditions on ionic Pt signal was equivalent to that previously shown for PtNPs signal (Fig. 1d–f). That is, ionic Pt signal decreased when increasing Q_g at low SD (*i.e.*, 4 mm) but it was enhanced at high SD (*i.e.*, 12 mm). In this case, however, it was observed that ionic Pt signal strongly depended on Q_l. Overall, it rose when increasing Q_l, regardless the Q_g and SD. Only when operating Q_g above 0.9 L min^{-1} and SD below 8 mm, there was no influence of Q_l on the ionic Pt signal.

To explain these findings, W_{ionic} was studied using the same experimental setup early employed with NPs (Fig. S3, ESI†). In agreement with previous findings for PtNPs, W_{ionic} was enhanced when increasing both Q_g and Q_l. Consequently, ionic Pt signal suppression noticed under some conditions (*e.g.*, 4 mm SD) was mostly related to a decrease on plasma atomization/ionization capabilities (Fig. 2).

As it has been previously noticed for PtNPs, changes on W_{ionic} with experimental conditions are different to those previously observed for S_{tot} thus providing different information about aerosol transport phenomena.[42] In general, it was observed that both W_{NP} and W_{ionic} responded similarly to changes on Q_g and Q_l. Nevertheless, signal spectra provided by PtNPs and ionic Pt show significant differences. When operating the PtNPs suspension, the number of pulses mostly depends on W_{NP} and to a lesser extent on instrument operating conditions (Fig. 1a–c). Signal intensity for PtNPs, however, only relies on the latter factor (Fig. 1d–f), and it is independent of aerosol transport. Alternatively, the ionic Pt signal simultaneously depend on both aerosol transport (S_{tot} and W_{ionic}) and

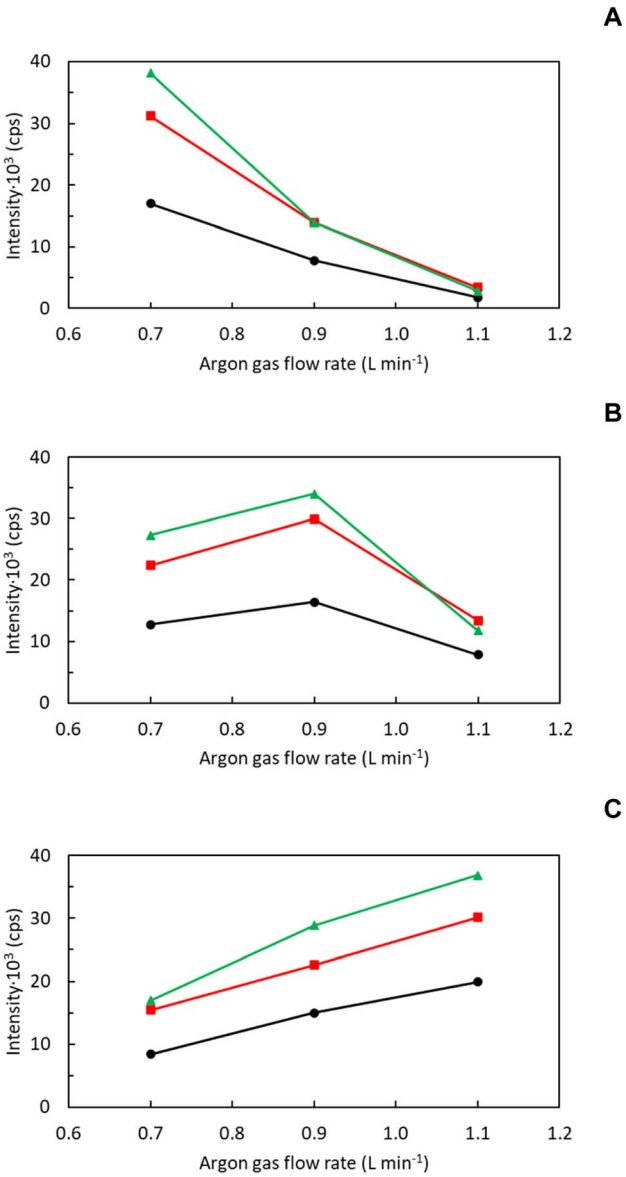

Fig. 3 Influence of the Q_g on the ionic Pt signal at different Q_l and SD. Q_l: 100 (-●-), 300 (-■-), and 500 µL min^{-1} (-▲-); SD: 4 (A), 8 (B) and 12 mm (C); R.f. power: 1550 W; ionic Pt concentration: 10 ng mL^{-1}.

operating conditions (Fig. 3).[3,15,31,32] This successfully explains why signal data for PtNPs and ionic Pt in ICP-MS look similar, but they are not totally equivalent.

3.3. Considerations about aerosol transport in spICP-MS

As it has been mentioned previously, in the absence of certified standards of known size and concentration, the appropriate characterization of a given NMs suspension relies on estimating NMs transport efficiency.[3,4,25,26] To this end, different strategies have been proposed based on measuring: (i) the number of events;[25] (ii) the ionic and NMs pulse intensity ratio;[25] and (iii) solvent transport efficiency.[25,28,29] Though these strategies have been indistinctively employed in the literature for NMs characterization,[1,4,27] only the first one is really based on NMs

transport through the sample introduction system. The remaining approaches provide an indirect estimate of NMs transport efficiency since they are based on ions and solvent transport rate. Consequently, these strategies cannot provide equivalent results to those obtained using the number of events unless NMs, ions and solvent do behave similarly through the sample introduction system and in the plasma. To gain insight into how these species behave through the sample introduction system, transport efficiency has been calculated for each of them from data gathered in Table 2. It must be considered that no direct comparison is feasible based on transport flow rate since the flux for each species is measured in different units. Table 3 shows transport efficiencies for PtNPs (η_{NP}), ionic Pt (η_{ionic}) and solvent (η_S) under different nebulization conditions (*i.e.*, Q_g and Q_l). Irrespective of the species considered, transport efficiency was mostly enhanced when increasing Q_g as well as when decreasing Q_l. These results were in agreement with previous reports in the literature[37,43] and it could be rationalized considering that, the higher the ratio between Q_g and Q_l, aerosols become finer, and they are more efficiently transported into the plasma. As it is shown in Table 3, there were significant differences on transport efficiency between all the species investigated. In general, for most of the conditions tested, η_S was the highest followed by η_{ionic} and η_{NP}. These results are not unexpected considering that η_S encompasses liquid and vapor solvent transport into the plasma, but the latter factor is not relevant for ionic Pt and PtNPs.[42] Interestingly, it was observed that differences on transport efficiency between the solvent and the remaining species were reduced when operating higher Q_g : Q_l ratios. While it is generally accepted that ions and NPs are transported similarly through the sample introduction system,[3,25] data shown in Table 3 suggest that there are indeed some differences between both species. In general, for most of the conditions tested, η_{ionic} was higher than η_{NP} and differences between both species were up to 16%. The origin of this bias is unclear, but it should be related to aerosol generation and transport processes (*i.e.*, NMs and ion distribution within aerosol droplets). Aerosols generated by pneumatic nebulizers do have a net electrical charge[44] and, hence, some aerosol transport phenomena (*e.g.*, Coulomb fission,[44] AIR effect,[45] *etc.*) might affect both species differently.

From the discussion above, it is clearly demonstrated that there are significant differences on NMs, ions and solvent transport efficiency. This means that NMs characterization will be critically dependent on the approach selected to assess this parameter. Hence, the influence of each strategy (*i.e.*, number of events, ionic and NMs signal ratio and solvent-based methodologies) on both PtNPs particle size and number concentration are covered in detail. Additionally, alternative NPs (*i.e.*, 50 and 150 nm AuNPs) and spray chamber design (*i.e.*, cyclonic) has also been tested to validate major experimental findings.

3.3.1. Transport efficiency calculated from the number of events. This strategy relies on NMs transport into the discharge and, hence, it is apparently the most suitable for the accurate characterization of unknown NMs suspensions provided they are stable, and no particles are lost prior to sample nebulization. To confirm this hypothesis, the (70 nm) PtNPs suspension was characterized by means spICP-MS under different operating conditions using this approach. To this end, a PtNPs suspension with a nominal concentration 1.5×10^4 mL^{-1} was initially employed for assessing transport efficiency. Next, a calibration with ionic standards was performed to relate PtNPs ionization signals with the mass of PtNPs and, considering particle density, with the volume.[25] For the sake of comparison, PtNPs were also characterized by means TEM and NMs transport efficiency was calculated with the aid of the filter-based methodology. Thus, it is feasible to evaluate whether NMs characterization is potentially biased due to either aerosol or plasma phenomena. Fig. 4 shows PtNPs particle size distributions for a Q_l of 300 μL min^{-1} under different Q_g (0.7/0.9/1.1 L min^{-1}) and SD (4/8/12 mm). Similar findings were found operating alternative Q_l (*i.e.*, 100/500 μL min^{-1}). Irrespective of the operating conditions, PtNPs mean diameter afforded by spICP-MS was equivalent to than found with TEM (*i.e.*, 70 ± 4 nm). However, it was observed that the particle size distributions afforded by the former technique were strongly dependent on the operating conditions. Thus, when operating a Q_g of 0.7 L min^{-1} and a Q_l of 300 μL min^{-1}, both spICP-MS and TEM particle size distribution were mostly indistinguishable, regardless the SD selected. Interestingly, under these conditions, transport efficiency by using the number of events (*i.e.*, 2.85–3.18%, depending on the selected SD) matches that found using air filters (Table 3). Size distributions by means spICP-MS were, however, severely broadened when increasing Q_g (*i.e.*, 0.9–1.1 L min^{-1}) as well as when decreasing SD (*i.e.*, 4 mm). In these conditions, SPAN (*i.e.*, width of particle size distributions[46]) increased up to 50%. These results are not unexpected considering that plasma characteristics are deteriorated (Fig. 2), and analyte diffusion within the plasma become more important (*i.e.*, ion clouds overlapping issues). In fact, when operating a Q_g of 1.1 mL min^{-1} and a SD of 4 mm, transport efficiency estimated by the number of event method (*i.e.*, 1.57 ± 0.07%) was severely biased (−40%) with that measured at the exit of the spray chamber with the aid of filters (Table 3). As with PtNPs, 50 nm (Fig. S5†) and 150 nm AuNPs (Fig. S6†) were characterized by means spICP-MS under different operating conditions using the number of events for transport efficiency assessment. Overall, experimental findings were like those found for PtNPs. Nevertheless, it was noticed that size distribution for the 150 nm were significantly broadened regarding TEM, irrespective of the experimental conditions tested. These results suggest that plasma-related phenomena affect differently 50 nm and 150 nm.[32]

Table 3 Influence of Q_g and Q_l on solvent, ionic Pt and PtNPs transport efficiency

Q_g (L min^{-1})	Q_l (μL min^{-1})	η_S (%)	η_{ionic} (%)	η_{NP} (%)
0.7	300	4.92 ± 0.05	2.99 ± 0.07	3.10 ± 0.06
0.9	100	10.4 ± 0.2	10.3 ± 0.2	8.9 ± 0.3
	300	5.77 ± 0.03	3.89 ± 0.12	3.35 ± 0.06
	500	4.12 ± 0.06	2.71 ± 0.11	2.10 ± 0.07
1.1	300	5.18 ± 0.09	4.9 ± 0.2	4.24 ± 0.04

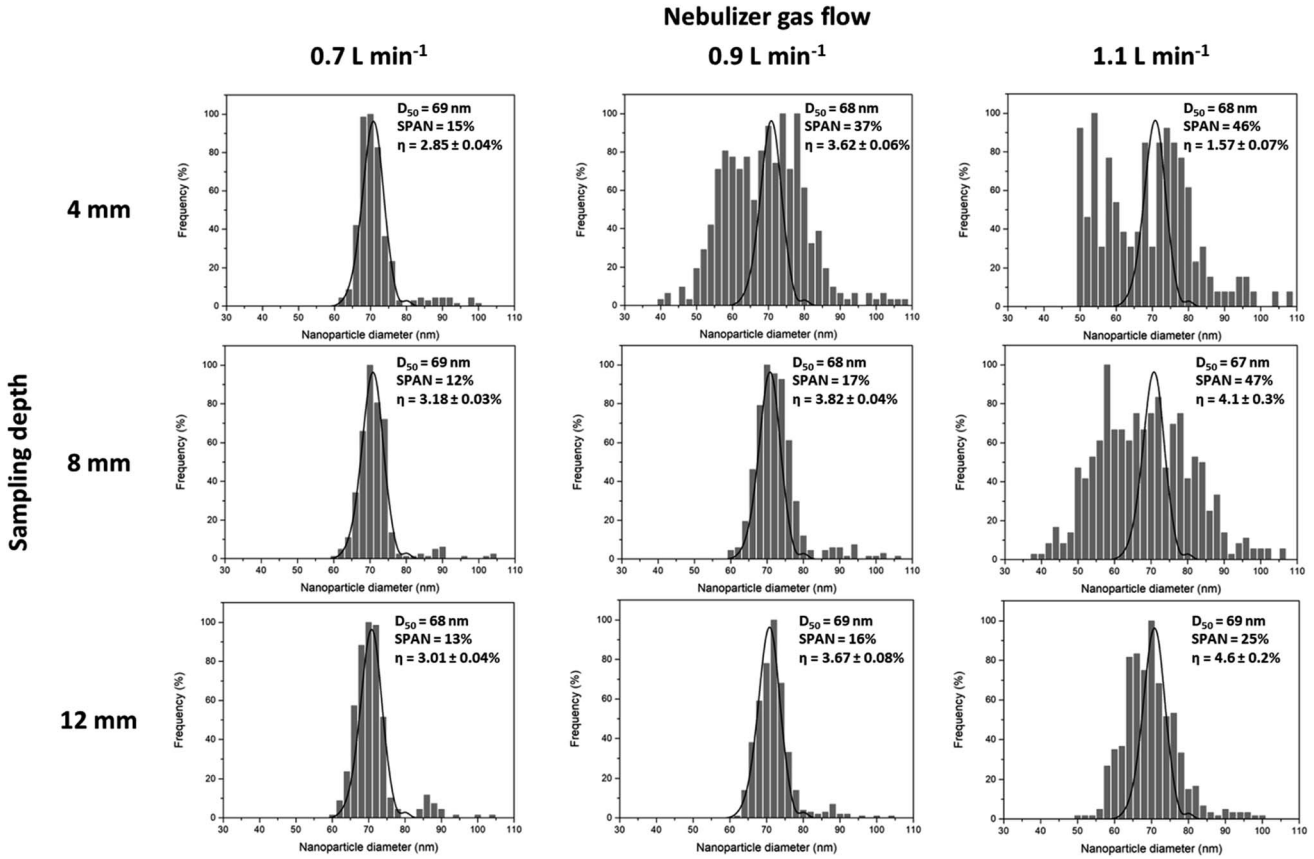

Fig. 4 Platinum NPs size distribution obtained using transport efficiencies calculated by means the number of events under different Q_g and SD. R.f. power 1550 W; Q_l 300 μL min^{-1}. PtNPs concentration: 1.5 × 10^4 mL^{-1}. Continuous line represents TEM particle size distribution.

From these results shown in this section, it is self-evident that the number of events provides an accurate assessment of NMs transport efficiency and, hence, NMs characterization. Nevertheless, special care should be required to ensure that a robust discharge is operated since otherwise biased results might be obtained.

3.3.2. Transport efficiency calculated from ionic and NMs pulse intensity. Several authors have reported that transport efficiencies estimated from ionic and NMs pulse intensity ratios are usually higher than those afforded by the number of events.[25,30] Different hypothesis have been considered for explaining these differences such as the lack of suspension stability or inappropriate dilution (high NM concentration levels) among others.[25,30] Nevertheless, according to our data, this bias could be explained considering the different behavior shown by NMs and ions in spICP-MS. As it was already noted by Pace *et al.*[25] when proposed this methodology, transport efficiency can only be estimated from the ratio of solution sensitivity and NPs sensitivity assuming equal transport efficiencies between particulate and dissolved solutions. Since this latter requirement appears to be broken under some experimental conditions, transport efficiency estimated by means this approach might not be equivalent to that obtained with the number of events.[4,27] In fact, as it has already noted (Fig. 1 and 3; Sections 3.1 and 3.2), ionic signal was more dependent on operating conditions than the signal generated by NMs ionization. Nanomaterials transport efficiency afforded by this approach was evaluated under different operating conditions and results were compared with those obtained using the number of events for assessing transport efficiency. Fig. 5 shows the relative transport efficiency (η_{rel}), defined as the ratio between the transport efficiency calculated for the number of events and ionic and NMs pulse intensity for PtNPs, under different Q_g and SD values for a fixed Q_l of 300 μL min^{-1}. If both strategies provide equivalent transport efficiencies, this ratio should be close to unity. Conversely, if the ionic and NMs pulse intensity approach provides higher transport efficiencies, this ratio will be lower than unity. As it can be observed in this figure, for all the conditions tested, η_{rel} was lower than unity thus indicating that the latter methodology overestimates PtNPs transport efficiency regarding the value obtained from the number of events (Fig. 5). For instance, when operating a Q_g of 0.9 L min^{-1} and a SD of 8 mm, bias on transport efficiency was close to +15%. Interestingly, the highest differences on η_{rel} were observed under non-robust conditions (*i.e.*, Q_g > 0.9 L min^{-1}; SD < 8 mm). Similar findings were noticed operating 50 and 150 nm AuNPs (Fig. S7†).

As expected, PtNPs size distribution calculated using transport efficiency from ionic and pulse intensity were significantly biased regarding those obtained with the number of events and

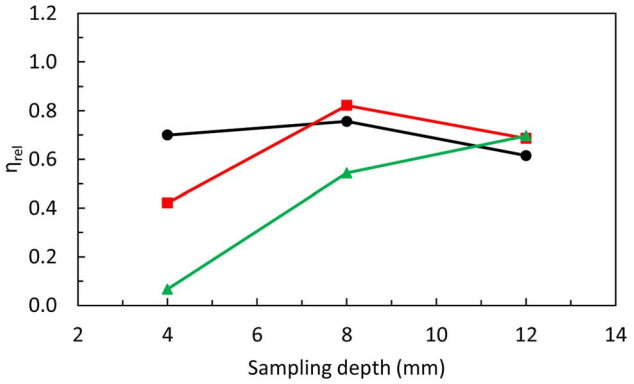

Fig. 5 Influence of the SD on the transport efficiency ratio between the number of events and ionic and NMs signal ratio methodologies (η_{rel}) operating different Q_g values. Q_g: 0.7 L min^{-1} (-●-), 0.9 L min^{-1} (-■-), and 1.1 L min^{-1} (-▲-). R.f. power: 1550 W; Q_l: 300 μL min^{-1}.

TEM (Fig. S8†). However, because the dampening effect of cubic root when calculating particle size using transport efficiency, bias on particle size distribution is less significant. Thus, under the above-mentioned conditions (Q_g of 0.9 L min^{-1} and SD of 8 mm), bias on the PtNPs mean size diameter was just 7%. As regards number concentration, since the use of ionic and NMs pulse intensity ratio overestimates NMs transport and this latter parameter is inversely proportional to transport efficiency, results will be negatively biased with regard the use of the number of events.[11] In this work, depending on operating conditions, concentration bias ranged from −95 to −15%.

In the light of above discussion, the use of ionic and NMs pulse intensity ratio for assessing transport efficiency is far from being an ideal methodology since it is based on several assumptions that are only fulfilled in certain conditions.

3.3.3. Transport efficiency calculated from solvent transport. Solvent-based methodologies have been proposed as an alternative to the above-mentioned approaches since they are traceable to the SI and does not require the use of a NMs reference suspension.[28] Nevertheless, because solvent-based strategies do not reflect how NMs are transported into the plasma, they are unsuitable for estimating NMs transport efficiency and, hence, their use are also discouraged. To the best of authors' knowledge, this strategy has not been employed for assessing transport efficiency with volatile solvents but it is expected that transport efficiency bias will be higher to that found in this work due to the higher solvent fraction transported in vapor phase.[20]

Platinum nanoparticles size distributions were calculated under different operating conditions (Fig. S9†) using this strategy (Table 3). In this case, solvent transport efficiency is fixed for a given set of Q_g and Q_l. As expected, PtNPs size distributions were biased up to +44% when operating this strategy. Interestingly, under certain conditions (Q_g 0.9 L min^{-1} and SD 12 mm), this approach might afford similar results to those obtained with TEM data and the frequency approach. Anyway, this fact does mean NMs and solvent transport efficiency are equivalent, particularly considering that bias on particle mean diameter is partially reduced due to the dampening effect of the cubic root when calculating particle size from transport efficiency. Finally, bias on number concentration ranged from −70 to −15%.[25]

3.3.4. Influence of spray chamber design on aerosol transport phenomena. Aerosol transport phenomena strongly depends on spray chamber characteristics[39] and, hence, it is important to evaluate whether previous findings are related to a specific spray chamber design. Therefore, additional experiments were carried out coupling the Micromist nebulizer to a cyclonic spray chamber. Overall, experimental findings for this setup were similar to those previously found with a double pass spray chamber. Thus, irrespective of experimental conditions, η_{ionic} was higher than η_{NP} and also transport efficiency values calculated from the number of events were systematically lower than those obtained using ionic and NMs pulse signals. For instance, when operating a Q_g of 0.9 L min^{-1}, 300 μL min^{-1} and a SD of 8 mm (CeO^+/Ce^+ ratio <2%), PtNPs transport efficiency calculated for both approaches were, respectively, 3.7 ± 0.2 and 5.0 ± 0.2. Due to these differences, particle mean (+15%) and concentration (−35%) for PtNPs was again biased. These results confirms than NMs and ions transport through the sample introduction system are not equivalent and the significance of selecting the appropriate strategy for assessing transport efficiency.

4. Conclusions

An in-depth characterization of tertiary aerosols reveals that NMs, ionic and solvent transport efficiency could differ significantly under standard spICP-MS operating conditions. This fact has significant practical implications since different strategies have been proposed for assessing NMs transport efficiency indirectly using either ionic or solvent transport. As long as a robust plasma is operated, transport efficiency can be accurately determined by measuring the number of events provided by a NMs suspension of known concentration. The use of ionic and NMs pulse intensity to estimate transport efficiency assumes that NMs and ions behave similarly through the sample introduction system and within the plasma, but these requirements are not always fulfilled. Therefore, special care is required if this strategy is used considering that transport efficiency assessment is strongly affected by plasma operating conditions. Finally, strategies based on measuring solvent transport efficiency as a proxy of NMs transport efficiency are not correct on the conceptual level and, hence, they should not be used.

It is the author's view that current knowledge about the role of aerosol transport phenomena in spICP-MS is still very limited thus negatively affecting technique metrology. So, further research efforts are clearly required in this area, particularly about how NMs coatings and matrix concomitants affect transport efficiency. In order to gain insight into aerosol transport phenomena, it is critical that future works explore this topic holistically since current focus have been exclusively centered in the plasma, being difficult to distinguish whether experimental findings are related to aerosol – and/or plasma – phenomena. On the other hand, because some relevant experimental details are not usually provided (*e.g.*, sampling depth, torch i.d., sample introduction system setup, plasma

robustness, *etc.*), it is quite challenging to compare results between different authors and, above all, replicate them.

Conflicts of interest

There are no conflicts to declare.

Acknowledgements

The authors would like to thank the Generalitat Valenciana (PROMETEO/2021/055) and the Vice-Presidency for Research and Knowledge Transfer of the University of Alicante for the financial support of this work (VIGROB-050). D. Torregrosa thanks the Spanish Ministerio de Ciencia, Innovación y Universidades for the fellowship FPU17/02853.

References

1 D. Mozhayeva and C. Engelhard, *J. Anal. At. Spectrom.*, 2020, **35**, 1740.
2 E. Bolea, M. S. Jimenez, J. Perez-Arantegui, J. C. Vidal, M. Bakir, K. Ben-Jeddou, A. C. Gimenez-Ingalaturre, D. Ojeda, C. Trujillo and F. Laborda, *Anal. Methods*, 2021, **13**, 2742.
3 F. Laborda, J. Jiménez-Lamana, E. Bolea and J. R. Castillo, *J. Anal. At. Spectrom.*, 2013, **28**, 1220.
4 M. D. Montaño, J. W. Olesik, A. G. Barber, K. Challis and J. F. Ranville, *Anal. Bioanal. Chem.*, 2016, **408**, 5053.
5 V. Kinnunen, S. Perämäki and R. Matilainen, *Spectrochim. Acta, Part B*, 2021, **177**, 106104.
6 I. Kálomista, A. Kéri and G. Galbács, *Talanta*, 2017, **154**, 147.
7 I. Abad-Álvaro, E. Peña-Vázquez, E. Bolea, P. Bermejo-Barrera, J. R. Castillo and F. Laborda, *Anal. Bioanal. Chem.*, 2016, **408**, 5089.
8 K.-S. Ho, W.-W. Lee and W.-T. Chan, *J. Anal. At. Spectrom.*, 2015, **30**, 2066.
9 I. Kálomista, A. Kéri, D. Ungor, E. Csapó, I. Dékány, T. Prohaska and G. Galbács, *J. Anal. At. Spectrom.*, 2017, **32**, 2455.
10 B. Franze, I. Strenge and C. Engelhard, *J. Anal. At. Spectrom.*, 2012, **27**, 1074.
11 J. Kocic, D. Günther and B. Hattendorf, *J. Anal. At. Spectrom.*, 2021, **36**, 233.
12 E. Bolea-Fernandez, D. Leite, A. Rua-Ibarz, T. Liu, G. Woods, M. Aramendia, M. Resano and F. Vanhaecke, *Anal. Chim. Acta*, 2019, **1077**, 95.
13 I. Kálomista, A. Kéri and G. Galbacs, *J. Anal. At. Spectrom.*, 2016, **31**, 1112.
14 E. Bolea-Fernández, D. Leite, A. Rua-Ibarz, T. Liu, T. G. Woods, M. Aramendia, M. Resano and F. Vanhaecke, *Anal. Chim. Acta*, 2019, **1077**, 95.
15 R. Peters, Z. Herrera-Rivera, A. Undas, M. van der Lee, H. Marvin, H. Bouwmeester and S. Weigel, *J. Anal. At. Spectrom.*, 2015, **30**, 1274.
16 M. Witzler, F. Kullmer and K. Gunther, *Anal. Lett.*, 2018, **51**, 587.
17 M. Loula, A. Kana and O. Mestek, *Talanta*, 2019, **202**, 565.
18 K. Mehrabi, D. Günther and A. Gundlach-Graham, *Environ. Sci.: Nano*, 2019, **6**, 3349.
19 S. Harycki and A. Gundlach-Graham, *Anal. Bioanal. Chem.*, 2022, **414**, 7543.
20 D. Torregrosa, C. Gómez-Pertusa, G. Grindlay, L. Gras and J. Mora, *J. Anal. At. Spectrom.*, 2023, **38**, 403.
21 Y. Huang, J. Tsz-Shan Lum and K. S. Y. Leung, *J. Anal. At. Spectrom.*, 2020, **35**, 2148.
22 M. Aramendía, J. C. García-Mesa, E. Vereda Alonso, R. Garde, A. Bazo, J. Resano and M. Resano, *Anal. Chim. Acta*, 2022, **1205**, 339738.
23 L. Hendriks, B. Ramkorun-Schmidt, A. Gundlach-Graham, J. Koch, R. N. Grass, N. Jakubowski and D. Günther, *J. Anal. At. Spectrom.*, 2019, **34**, 716.
24 X. Tian, H. Jiang, M. Wang, W. Cui, Y. Guo, L. Zheng, L. Hu, G. Qu, Y. Yin, Y. Cai and G. Jiang, *Anal. Chim. Acta*, 2023, **1240**, 340756.
25 H. E. Pace, N. J. Rogers, C. Jarolimek, V. A. Coleman, C. P. Higgins and J. F. Ranville, *Anal. Chem.*, 2011, **83**, 9361.
26 O. Geiss, I. Bianchi, G. Bucher, E. Verleysen, F. Brassinne, J. Mast, K. Loeschner, L. Givelet, F. Cubadda, F. Ferraris, A. Raggi, F. Iacoponi, R. Peters, A. Undas, A. Müller, A. Meinhardt, B. Hetzer, V. Gräf, A. R. Montoro Bustos and J. Barrero-Moreno, *Nanomaterials*, 2022, **12**, 725.
27 M. Resano, M. Aramendía, E. García-Ruiz, A. Bazo, E. Bolea-Fernández and F. Vanhaecke, *Chem. Sci.*, 2022, **13**, 4436.
28 S. Cuello-Nuñez, I. Abad-Álvaro, D. Bartczak, M. E. del Castillo Busto, D. A. Ramsay, F. Pellegrino and H. Goenaga-Infante, *J. Anal. At. Spectrom.*, 2020, **35**, 1832.
29 J. Tuoriniemi, G. Cornelis and M. Hassellöv, *J. Anal. At. Spectrom.*, 2014, **29**, 743.
30 J. Liu, K. E. Murphy, M. R. Winchester and V. A. Hackley, *Anal. Bioanal. Chem.*, 2017, **409**, 6027.
31 J. W. Olesik and P. J. Gray, *J. Anal. At. Spectrom.*, 2012, **27**, 1143.
32 W.-W. Lee and W.-T. Chan, *J. Anal. At. Spectrom.*, 2015, **30**, 1245.
33 G. Grindlay, J. Mora, M. T. C. de Loos-Vollebregt and F. Vanhaecke, *Spectrochim. Acta, Part B*, 2013, **86**, 42.
34 M. C. García-Poyo, G. Grindlay, L. Gras, M. T. C. de Loos-Vollebregt and J. Mora, *Spectrochim. Acta, Part B*, 2015, **105**, 71.
35 D. Torregrosa, G. Grindlay, M. de la Guardia, L. Gras and J. Mora, *Talanta*, 2023, **252**, 123818.
36 G. Grindlay, L. Gras, J. Mora and V. Hernandis, *J. Anal. At. Spectrom.*, 2008, **23**, 129.
37 R. F. Browner, A. Canals and V. Hernandis, *Spectrochim. Acta, Part B*, 1992, **47**, 659.
38 G. Grindlay, S. Maestre, J. Mora, V. Hernandis and L. Gras, *J. Anal. At. Spectrom.*, 2005, **20**, 455.
39 J. Mora, S. Maestre, V. Hernandis and J. L. Todolí, *TrAC, Trends Anal. Chem.*, 2003, **22**, 123.
40 J. Mora, J. L. Todolí, A. Canals and V. Hernandis, *J. Anal. At. Spectrom.*, 1997, **12**, 445.
41 A. Montaser, M. G. Minnich, H. Liu, A. G. T. Gustavsson and R. F. Browner, in *Inductively Coupled Plasma Mass*

Spectrometry, ed. A. Montaser, Wiley-VCH, New York, 1998, pp. 335–420.
42 D. D. Smith and R. F. Browner, *Anal. Chem.*, 1982, **54**, 533.
43 A. Canals, V. Hernandis and R. F. Browner, *Spectrochim. Acta, Part B*, 1990, **45**, 591.
44 M. W. Tessum and P. C. Raynor, *J. Aerosol Sci.*, 2021, **151**, 105691.
45 J. L. Todolí, L. Gras, V. Hernandis and J. Mora, *J. Anal. At. Spectrom.*, 2002, **17**, 142.
46 H. Moghadam, M. Zakeri and A. Samimi, *J. Part. Sci. Technol.*, 2019, **5**, 71.